Identification of the silver state in the framework of Ag-containing zeolite by XRD, FTIR, photoluminescence, 109 Ag NMR, EPR, DR UV-vis, TEM and XPS investigations

Nataliia Popovych, Pavlo Kyriienko, Sergiy Soloviev, Rafal Baran, Yannick Millot, Stanislaw Dzwigaj

Identification of the silver state in the framework of Ag-containing zeolite by XRD, FTIR, photoluminescence, ^{109}Ag NMR, EPR, DR UV-vis, TEM and XPS Investigations

Nataliia Popovych[a], Pavlo Kyriienko[a], Sergiy Soloviev[a], Rafal Baran[b,c] ,

Yannick Millot[c] and Stanislaw Dzwigaj[c,*]

[a]L.V.Pisarzhevsky Institute of Physical Chemistry of the NAS of Ukraine,

31 Prosp. Nauky, 03028 Kyiv, Ukraine

[b]AGH University of Science and Technology al. A. Mickiewicza 30, 30-059 Krakow, Poland

[c]Sorbonne Universités, UPMC Univ Paris 06, CNRS, UMR 7197, Laboratoire de Réactivité de Surface, 4 place Jussieu, F-75252, Paris, France

Figures: 13

Keywords: Silver, zeolite, postsynthesis, NMR, EPR, photoluminescence

*Corresponding author

Stanislaw Dzwigaj, e-mail : stanislaw.dzwigaj@upmc.fr, fax : +33 1 44 27 21 13

Abstract

Silver has been identified in the framework of Ag_xSiBEA zeolites (where x = 3 - 6 Ag wt %) by combined use of XRD, ^{109}Ag MAS NMR, FTIR, diffuse reflectance UV-visible, EPR and XPS. The incorporation of Ag ions into the framework of SiBEA zeolite has been evidenced by XRD. The consumption of OH groups as a result of their reaction with silver precursor has been monitored by FTIR and photoluminescence. The changes of the silver state as a function of Ag content, thermal and hydrogen treatment at 573 K have been identified by ^{109}Ag MAS NMR, EPR, DR UV-visible, TEM and XPS. The acidity of AgSiBEA has been investigated by FTIR spectroscopy of adsorbed CO and pyridine used as probe molecules.

1. Introduction

In recent years, increasing attention has been focused on the introduction of transition metals into zeolites and the use of the resulting materials as catalysts for various types of reactions. Zeolites containing transition metals are known to be efficient catalysts for selective catalytic reduction (SCR) of NO with different reducing agents [1-5], selective oxidation of methanol [6], oxidative dehydrogenation of propane [7,8], oxidation of CO [9], hydrodechlorination of chloroorganic compounds, hazardous pollutants of natural environment [10] or Fischer-Tropsch reaction of syngas to liquid hydrocarbons [11]. Catalysts based on BEA zeolites are widely investigated for industry processes and environmental protection due their high activity [5,12-14].

Interest in Ag-containing catalysts for the selective catalytic reduction of NO_x was heightened after the finding that addition of hydrogen into the reaction mixture enhances the conversion of nitrogen oxide [15-18]. However, there is still lack of data in the literature concerning application of silver-containing zeolites in the SCR of NO_x. According to previous reports, dispersed silver species seem to be active catalytic centers of SCR of NO on Ag-MFI zeolites [18,19]. However, silver is not well dispersed in such materials, which contain silver in the form of various species, *i.e.*, ions, nanoclusters, and metallic nanoparticles. Moreover, stabilization of silver in different oxidation states (Ag^+ and Ag^{2+}) may result in higher catalytic activity of Ag-containing catalysts, as was shown earlier for $Sr_{1-x}Ag_xTiO_{3\pm\delta}$ perovskites [20]. Ag^{2+} ions, substituting part of Sr^{2+} in the lattice, could interact with some O_x^- species, leading to O_x^-/Ag^{2+} couples and so influencing oxygen mobility and catalytic activity.

To obtain well-dispersed silver species and to identify their state a two-step postsynthesis method was used, which developed earlier for preparation of metal-containing BEA zeolites [21,22]. This postsynthesis procedure allowed, for low metal content,

incorporating of silver ions in the framework of zeolite mainly as isolated mononuclear silver species without formation of metal oligomers or metal oxides [23].

In the present work, we have identified silver state in the framework of Ag-containing BEA zeolites after different treatments using different physicochemical techniques such ^{109}Ag MAS NMR, EPR, UV-visible diffuse reflectance, and XPS.

2. Experimental section

2.1. Materials

TEABEA zeolite provided by RIPP (China) was treated in a 13 mol·L^{-1} HNO_3 aqueous solution (4 h, 353 K) to obtain a dealuminated and organic-free SiBEA support (Si/Al =1000) with the vacant T-atom sites. SiBEA was then washed with distilled water and dried at 353 K. To incorporate Ag ions in the vacant T-atom sites two-step postsynthesis method were applied, described in our earlier report [23]. 2 g of SiBEA was firstly stirred under aerobic conditions for 2 h at 298 K in 200 mL of $AgNO_3$ aqueous solution (pH = 2.3) with two concentration of 5.4 and 10.8 × 10^{-3} mol·L^{-1}. Then, the suspensions were stirred in evaporator under vacuum of a water pump for 2 h in air at 353 K until the water was evaporated. The resulting solids containing 3.0 and 6.0 Ag wt. % were labeled as $Ag_{3.0}$SiBEA and $Ag_{6.0}$SiBEA, respectively.

The as prepared Ag-containing SiBEA materials were calcined at 773 K (100 K h^{-1}) over 3 h and denoted as C-$Ag_{3.0}$SiBEA and C-$Ag_{6.0}$SiBEA. The materials were reduced in flowing H_2 (100 mL min^{-1}) at 573 K for 1h and denoted as Red-C-$Ag_{3.0}$SiBEA and Red-C-$Ag_{6.0}$SiBEA.

2.2. Techniques

X-ray fluorescence chemical analysis was performed at room temperature on SPECTRO X-LabPro apparatus.

XRD experiments were done on a PANalytical Empyrean diffractometer equipped with the Cu Kα radiation (λ = 154.05 pm) in the 2θ range of 5°−90°.

The stationary photoluminescence spectra were recorded on a Perkin-Elmer LS55 luminescence spectrometer at room temperature under ambient condition. The samples were excited with light of 250 nm. The excitation spectra were taken at 400 nm.

DR UV–vis spectra were recorded under ambient conditions on a Specord M40 (Carl Zeiss) with a standard diffuse reflectance unit.

X-ray photoelectron spectroscopy (XPS) measurements were performed with a hemispherical analyzer (PHOIBOS 100, SPECS Gmbh) using MgK_{α} (1253.6 eV) radiation. The power of the X-ray source was 300 W. The area of the sample analyzed was ~ 3 mm^2. The powder samples were pressed on an indium foil and mounted on a special holder. Binding energy (BE) for Si and Ag was measured by reference to the O 1s peak at 532.5 eV, corresponding to the binding energy of oxygen bonded to silicon. Before analysis, samples were outgassed at room temperature to a pressure of 10^{-7} Pa. All spectra were fitted with a Voigt function (a 70/30 composition of Gaussian and Lorentzian functions) in order to determine the number of components under each XPS peak.

^{109}Ag NMR spectra were recorded with a Bruker Avance 700 spectrometer at 32.74 MHz and with a low-frequency 4-mm CP/MAS probe. The spinning speed was 14 kHz. To eliminate acoustic ringing artifacts, the spectra were acquired with spin-echo pulse sequence ($\pi/2-\tau-\pi-\tau$), a $\pi/2$ pulse duration of 10 μs and 10 s for recycle delay. Between 30000 to 50000 transients were acquired for each spectrum. Chemical shifts of silver were measured by reference to $AgSO_3CH_3$ (δ = 87.2 ppm) [24].

EPR spectra were recorded on a JEOL FA-300 series EPR spectrometer at 9.3 GHz (X band) using a 100 kHz field modulation and a 5−10 G standard modulation width. The spectra were recorded at 298 and 77 K for fresh, calcined and reduced samples. The fresh $Ag_{3.0}$SiBEA and $Ag_{6.0}$SiBEA samples were calcined at 773 K for 2 h under a dynamic vacuum of 10^{-3} Pa at which led to the activated C-$Ag_{3.0}$SiBEA and C-$Ag_{6.0}$SiBEA samples, respectively. Then C-$Ag_{3.0}$SiBEA and C-$Ag_{6.0}$SiBEA samples were reduced by treatment with pure H_2 at 573 K for 1 h what led to the Red-C-$Ag_{3.0}$SiBEA and Red-C-$Ag_{6.0}$SiBEA samples.

TEM micrographs were obtained on SELMI TEM-125K microscope operating at 100 kV. For TEM measurements a sample was dispersed in acetone with ultrasound and deposited on Cu grid covered with carbon. Interplanar spacings (d_{hkl}) calculated from the diffraction ring pattern were compared with ASTM data.

Analysis of the acidic properties of samples was performed by adsorption of CO or pyridine followed by infrared spectroscopy. Before analysis, the samples were pressed at ~ 1 ton·cm^{-2} into thin wafers of ca. 10 mg·cm^{-2} and placed inside the IR cell.

Before CO adsorption experiment, the wafers were activated by calcination at 723 K for 2 h in flowing 2.5 % O_2/Ar and then outgassed at 573 K (10^{-3} Pa) for 1 h. Following thermal treatment, the samples were cooled down to 100 K. CO was introduced in increasing amounts up to an equilibrium pressure of 133 Pa. Infrared spectra were recorded using a Bruker Vertex 70 spectrometer (resolution 2 cm^{-1}, 128 scans). The spectra were obtained after subtraction of the spectrum recorded after calcination and prior to CO adsorption.

Before pyridine adsorption/desorption experiments, the wafers were activated by calcination in static conditions at 773 K for 1 h in O_2 ($2 \cdot 10^4$ Pa) and then outgassing under secondary vacuum at 673 K (10^{-3} Pa) for 1 h. These wafers were contacted at 423 K with gaseous pyridine. The spectra were recorded after pyridine desorption at 423 K using a Spectrum One FTIR spectrometer (resolution 2 cm^{-1}, 24 scans). The reported spectra were

obtained after subtraction of the spectrum recorded after calcination and prior to pyridine adsorption and recalculated to a "normalized" wafer of 1 mg.

3. Results and discussion

3.1. Incorporation of Silver into SiBEA framework proved by XRD, FTIR and photoluminescence

An analysis of zeolite BEA structure modifications may be done by XRD involving monitoring of the main reflection peak at 2θ = 22.3°−22.6°, corresponding to d_{302} spacing, within a given series of zeolite samples. The d_{302} spacing for all studied samples was calculated from the corresponding 2θ value. The d_{302} spacing decreased from 3.979 Å for TEABEA to 3.921 Å for SiBEA indicating a matrix contraction, consistent with the removal of Al atoms from zeolite BEA structure. The introduction of Ag into SiBEA resulted in the increase of the d_{302} spacing from 3.921 Å (SiBEA) with 2θ of 22.60° to 3.950 Å ($Ag_{3.0}$SiBEA) with 2θ of 22.49° and to 3.945 Å ($Ag_{6.0}$SiBEA) with 2θ of 22.51° (**Figure 1**). Those changes in the position of the main diffraction peak suggest expansion of the BEA structure and the incorporation of silver ions into the vacant T–atom sites forming isolated, mononuclear Ag(I) species in line with our earlier reports on VSiBEA [22] and MoSiBEA [25] zeolites. Furthermore, all diffractograms are typical of zeolite BEA phase with no proofs of the structure amorphization and appearance of other crystalline phases, suggesting that the removal of aluminum by nitric acid treatment did not damage zeolite structure.

The FTIR spectra of SiBEA and $Ag_{6.0}$SiBEA are shown in the **Figure 2**. The incorporation of silver into SiBEA leads to the almost total disappearance of the IR bands at 3739, 3715 and 3533 cm^{-1} of isolated internal, terminal internal and hydrogen bonded SiOH groups (Figure 2), suggesting that these silanol groups reacted with the Ag precursor. After

incorporation of Ag ions in the vacant T-atom sites only the bands at 3752 cm^{-1} of isolated external silanol groups and the band at 3715 cm^{-1} of terminal internal silanol groups with very low intensity and the shoulder at 3740 cm^{-1} of isolated internal silanol groups are only present in $Ag_{6.0}$SiBEA (see inset in Fig. 2).

The incorporation of Ag^{+} ions into the vacant T-atom sites of the framework of BEA zeolite is confirmed by the photoluminescence spectroscopy. Figure 3 and 4 shows both photoluminescence and the excitation spectra of SiBEA and $Ag_{3.0}$SiBEA. The excitation spectrum of SiBEA exhibits broad band at about 249 nm with a shoulder at 262 nm (Fig. 4). They correspond to intense emission broad bands with maximum at about 400 and 645 nm (Fig. 3). The spectral distribution of the SiBEA photoluminescence obtained at 249 nm excitation light shown in **Figure 3** is very similar to that recently reported for siliceous MCM-41 and amorphous silica [26]. The emission bands at 400 and 645 nm are likely due to surface defects associated with SiO- and/or SiOH groups, in agreement with earlier reported data [27]. After incorporation of Ag ions in the SiBEA zeolite the intensity of the emission bands at 400 and 645 nm is strongly decreased (see the emission bands in Fig. 3 for $Ag_{3.0}$SiBEA) which confirm the reaction of Ag^{+} ions with silanol groups of vacant T-atom sites. Simultaneously, the intensity of the bands at 249 and 262 nm on excitation spectrum monitored at 400 nm of emission light are also strongly decreased (**Fig. 4**).

3.2 Nature of the silver in AgSiBEA zeolites evidenced by ^{109}Ag MAS NMR, EPR DR UV-Vis and XPS

The ^{109}Ag MAS NMR, EPR, DR UV-vis and XPS have been used to determine the nature of the silver in AgSiBEA zeolites.

^{109}Ag MAS NMR of $Ag_{3.0}$SiBEA, $Ag_{6.0}$SiBEA and Red-C-$Ag_{6.0}$SiBEA are given in **Fig. 5**. For $Ag_{3.0}$SiBEA only one silver signal is detected at 21.5 ppm indicating the formation

of only one main silver species in this sample, probably as isolated framework mononuclear Ag(I). The similar signal with chemical shift close to 20 ppm has been earlier observed by Pavlovskaya at al. [27] for different Ag-containing zeolites.

For the sample with much higher Ag content ($Ag_{6.0}$SiBEA) the one signal with chemical shift at –33.2 ppm appears. A decrease of the chemical shift with the Ag content could be explained by the formation of bigger $Ag_n^{\delta+}$ clusters with paramagnetic character. It is well know that silver clusters could have different magnetic properties, in particular paramagnetic ones [28-36] that could modify chemical shift of the NMR signal, in line with the earlier reports on paramagnetic shift [37-40]. The paramagnetic character of $Ag_n^{\delta+}$ clusters present in as prepared $Ag_{6.0}$SiBEA has been confirmed by EPR investigation (**Fig. 7**). The EPR spectrum of as prepared $Ag_{3.0}$SiBEA do not show any signal (**Fig. 6**), in contrast the EPR spectrum of as prepared $Ag_{6.0}$SiBEA reveals the presence of paramagnetic signal with low intensity with g= 2.00068 (Fig. 7).

The modification of the Ag species with increase of the Ag content has been confirmed by DR UV-vis investigation of as prepared $Ag_{3.0}$SiBEA and $Ag_{6.0}$SiBEA (**Fig. 8**). Both samples exhibit the band at 245 nm attributed to the charge transfer transition between $4d^{10}$ and $4d^9 5s^1$ levels of highly dispersed Ag(I) species (Fig. 8), in line with earlier reports [41-48]. The band at 245 nm for as prepared $Ag_{6.0}$SiBEA is more pronounced than that for as prepared $Ag_{3.0}$SiBEA. Probably, this is related with the presence in the former ones of much bigger amount of isolated $Ag_n^{\delta+}$ clusters. Two bands at 208 and 272-300 nm observed for both as prepared $Ag_{3.0}$SiBEA and $Ag_{6.0}$SiBEA are probably related to charge transfer transition in BEA framework observed also for silver-free SiBEA, as we have reported earlier [49].

Figure 9 shows the Ag $3d_{3/2}$ and $3d_{5/2}$ bands of calcined C-$Ag_{3.0}$SiBEA and C-$Ag_{6.0}$SiBEA. One peak at binding energy (BE) of 373.4 – 373.6 eV (Ag $3d_{3/2}$) and of 367.4 – 367.6 eV (Ag $3d_{5/2}$) indicates that Ag(I) species is the main silver species in both calcined C-$Ag_{3.0}$SiBEA and C-$Ag_{6.0}$SiBEA, in line with our earlier report [49].

After reduction of C-$Ag_{3.0}$SiBEA and C-$Ag_{6.0}$SiBEA the new phases are observed in XRD patterns of Red-C-$Ag_{3.0}$SiBEA and Red-C-$Ag_{6.0}$SiBEA with diffraction peaks at 2θ values of 38.10, 44.30, 64.30 and 77.28, which correspond to the (111), (200), (220) and (311) lattice planes of the face–centered cubic metallic silver (JCPDS: 03-065-2871) (Fig. 1). The very similar diffraction peaks have been reported earlier for Ag-SBA-15 obtained by direct synthesis [50].

After reduction of C-$Ag_{6.0}$SiBEA sample a knight shift of the NMR signal is observed for Red-C-$Ag_{6.0}$SiBEA (Fig.5), arisen from the interaction with the conduction electrons [51]. The signal recorded at 5272 ppm (Fig. 5) is associated with the presence of metallic nanoparticles, in line with earlier reports [27,52,53]. This is confirmed by DR UV-vis band at 375 nm for Red-C-$Ag_{3.0}$SiBEA and Red-C-$Ag_{6.0}$SiBEA (Fig. 8) and EPR signal of C-$Ag_{6.0}$SiBEA at g = 2.00159 and Red-C-$Ag_{6.0}$SiBEA at g = 2.00155 characteristic for silver nanoparticles (Fig. 7) [42,45,47]. The metallic nanoparticles are also formed in Red-C-$Ag_{3.0}$SiBEA as shown by the DR UV-vis band at 375 nm (Fig. 8) and in C-$Ag_{3.0}$SiBEA and Red-C-$Ag_{3.0}$SiBEA as shown by EPR signal at g = 2.00154 and at g = 2.00125 characteristic for silver nanoparticles (Fig. 6) with much lower amount than that observed for C-$Ag_{6.0}$SiBEA and Red-C-$Ag_{6.0}$SiBEA (Fig. 7).

Nanoparticles of silver with the average size of 10 nm were detected on TEM images of Red-C-$Ag_{3.0}$SiBEA zeolite (**Fig. 10**). Diffraction rings with d_{hkl} equal to 3.945, 2.044 and 1.183 Å can be respectively assigned to d_{302} spacing of BEA zeolite and (200), (222) planes of the face-centered cubic metallic silver.

3.3. FTIR characterization of acidic centres: adsorption of CO and pyridine

To determine the acidity of $Ag_{6.0}$SiBEA zeolites, the adsorption of CO and pyridine as probe molecules has been performed. The CO adsorption experiments give information on Bronsted acidity related to OH groups as well as on the nature and strength of Lewis acidic sites related to Al and Ag ions [54].

Difference spectra between FTIR spectra recorded after and before CO adsorption on $Ag_{6.0}$SiBEA at 100 K are given in Figs 11 and 12. For $Ag_{6.0}$SiBEA the adsorption of CO at 100 K leads to the appearance of only one main positive FTIR band at 3650 cm^{-1} and two negative bands at 3752 and 3715 cm^{-1} (Fig. 11). The 3752 and 3715 cm^{-1} bands correspond to isolated external and isolated internal Si-OH groups. A very small shift from 3752 to 3650 cm^{-1} (102 cm^{-1}) for isolated external Si-OH groups indicates that this silanol groups have a very weak acidic character.

FTIR spectra of CO adsorbed on $Ag_{6.0}$SiBEA (Fig. 12) exhibit in the carbonyl region narrow and well-resolved bands in the 2050-2250 cm^{-1} range. For $Ag_{6.0}$SiBEA, in CO equilibrium, the main bands appear at 2135, 2138, 2142, 2159, 2170 and 2189 cm^{-1}. However, after outgassing of the sample (10^{-3} Pa), the main IR band appears at 2170 cm^{-1} (see inset in Fig. 12) that could be assigned to CO bonded to mononuclear Ag(I) species, in line with earlier report on Ag-zeolites [54,55] and Ag/SiO_2 [56]. The ν(CO) stretching vibration of Ag^+-CO complexes, observed within the 2200-2150 cm^{-1} spectral range, depends on the type of the support, The carbonyls on Ag^+/SiO_2 are characterized by ν(CO) at 2169 cm^{-1} [56]. This value is close to that observed for CO adsorbed on $Ag_{6.0}$SiBEA sample.

The absence of the band at 3609 cm^{-1} in the IR spectrum of $Ag_{6.0}$SiBEA (Fig. 2) characteristic of acidic bridging Si-O(H)-Al groups confirm that absorption band at 2170 cm^{-1} is only due to CO bonded to mononuclear Ag(I) species.

The acidity of SiBEA, $Ag_{3.0}$SiBEA and $Ag_{6.0}$SiBEA was also investigated by FTIR spectroscopy with adsorption of pyridine on the samples calcined at 773 K (Fig. 13). The bands at 1600 and 1448 cm^{-1} appear for SiBEA related to pyridine interacting with weak Lewis acidic sites and/or pyridine physisorbed [57,58]. The incorporation of silver in SiBEA leads to appearance of new bands at 1605 and 1450 cm^{-1}, suggesting the formation of new silver Lewis acidic sites, as was shown earlier for $Ag_{1.5}$SiBEA zeolite [23]. The formation of silver LAS in zeolites may occur due to the interaction of silver with the gas phase oxygen. Adsorbed oxygen in this case is a conjugated base, i.e. Lewis conjugated acid-base pairs are formed on the oxidized silver species. Appearance of similar bands (1605 and 1450 cm^{-1}) has been earlier observed for AgHZSM-5 zeolites prepared by ion-exchange [59,60] and was assigned to pyridine adsorbed on silver species (Ag^+ or Ag_n^+).

The intensity of the bands corresponding to silver Lewis acidic sites grows with increasing Ag content, which may indicate higher amount of isolated mononuclear Ag(I) species incorporated in the zeolite framework for $Ag_{6.0}$SiBEA.

Conclusions

The two-step postsynthesis method used in preparation of AgSiBEA zeolites allowed incorporation of silver ions in the framework of BEA zeolite as isolated mononuclear Ag(I) species.

Silver has been identified in the framework of Ag_xSiBEA zeolites (where x = 3 - 6 Ag wt %) by combined use of XRD, ^{109}Ag MAS NMR, diffuse reflectance UV-visible, EPR and XPS.

The incorporation of Ag ions into framework of SiBEA zeolite has been evidenced by XRD by monitoring of the main reflection peak at $2\theta = 22.3°-22.6°$, corresponding to d_{302} spacing.

The consumption of OH groups as a result of their reaction with silver precursor has been monitored by FTIR and photoluminescence.

^{109}Ag MAS NMR, EPR, DR UV-visible, TEM and XPS allowed identifying the changes of the silver state as a function of Ag content, thermal and hydrogen treatment at 573 K. To the best of our knowledge, this is the first time that changes of silver state in the zeolite structure have been determined using simultaneously ^{109}Ag MAS NMR, EPR and DR UV-visible spectroscopies.

The acidity of AgSiBEA has been investigated by FTIR spectroscopy of adsorbed CO and pyridine used as probe molecules.

References

[1] P.S. Metkar, M.P. Harold, V. Balakotaiah, Appl. Catal. B 2012, **111-112**, 67-80.

[2] P. S. Metkar, M. P. Harold, V. Balakotaiah, Chem. Eng. Sci. 2013, **87**, 51-66.

[3] O. Krocher, M. Elsener, Ind. Eng. Chem. Res. 2008, **47**, 8588-8593.

[4] B. Gil, J. Janas, E. Wloch, Z. Olejniczak, J. Datka, B. Sulikowski, Catal. Today 2008, **137**, 174-178.

[5] J. Janas, S. Dzwigaj, Catal. Today 2011, **176**, 272-276.

[6] M. Trejda, M. Ziolek, Y. Millot, K. Chalupka, M. Che, S. Dzwigaj J. Catal. 2011, **281**, 169-176.

[7] A.K. Chalupka, C. Thomas, Y. Millot, F. Averseng, S. Dzwigaj, J. Catal. 2013, 305, 46-55.

[8] J. Janas, J. Gurgul, R.P. Socha, J. Kowalska, K. Nowinska, T. Shishido, M. Che, S. Dzwigaj, J. Phys. Chem. C 2009, **113**, 13273-13281.

[9] I. Kocemba, J. Rynkowski, J. Gurgul, R.P. Socha, K. Latka, J. M. Krafft, S. Dzwigaj, Appl. Catal. B 2016, **519**, 16-26

[10] A. Śrębowata, I. Zielińska, R. Baran, G. Słowik, S. Dzwigaj. Catal. Commun. 2015, **69**, 154–160.

[11] K. A. Chalupka, S. Casale, E. Zurawicz, J. Rynkowski, S. Dzwigaj, Micropor. Mesopor. Mater. 2015, **211**, 9-18.

[12] S. Dzwigaj, J. Janas, T. Machej, M. Che, Catal. Today 2007, **119** 133-136.

[13] J. Janas, T. Machej, J. Gurgul, L.P. Socha, M. Che, S. Dzwigaj, Appl. Catal. B 2007, **75** 239-248.

[14] J. Janas, J. Gurgul, R.P. Socha, S. Dzwigaj, Appl. Catal. B 2009, **91**, 217-224.

[15] S. Satokawa, Chem. Lett. 2000, **29**, 294-295.

[16] J.P. Breen, R. Burch, C.J. Hill, Catal. Today 2009, **145**, 34–37.

[17] N.O. Popovych, P.I. Kyriienko, S.O. Soloviev, S.M. Orlyk, S. Dzwigaj, Micropor. Mesopor. Mater. 2016, **226**, 10-18.

[18] J. Shibata, K. Shimizu, Y. Takada, A. Shichi, H. Yoshida, S. Satokawa, A. Satsuma, T. Hattori, J. Catal. 2004, **227**, 367–374.

[19] K. Shimizu, K. Sugino, K. Kato, S. Yokota, K. Okumura, A. Satsuma, J. Phys. Chem. C 2007, **111**, 1683–1688.

[20] L. Fabbrini, A. Kryukov, S. Cappelli, G.L. Chiarello, I. Rossetti, C. Oliva, L. Forni, J. Catal. 2005, **232**, 247-256.

[21] S. Dzwigaj, M.J. Peltre, P. Massiani, A. Davidson, M. Che, T. Sen, S. Sivasanker, Chem. Commun. 1998, 87-88.

[22] S. Dzwigaj, Curr. Opin. Solid State Mater. Sci. 2003, **7**, 461.

[23] S. Dzwigaj, Y. Millot, J-M. Krafft, N. Popovych, P. Kyriienko, J. Phys. Chem. C 2013, **117**,12552.

[24] G. H. Penner and W. Li, Inorg. Chem. 2004, **43**, 5588-5597.

[25] R. Baran, F. Averseng, Y. Millot, T. Onfroy, S. Casale and S. Dzwigaj, J. Phys. Chem. C, 2014, **118**, 4143–4150.

[26] M.E. Gimon-Kinsel, K. Groothuis, K.J. Balkus, Micropor. Mesopor. Mater. 1998, **20**, 67-76.

[27] G. E. Pavlovskaya, C. F. Horton-Garcia, C. Dybowski, D. R. Corbin and T. Meersmann, J. Phys. Chem. B, 2004, **108**, 1584-1589.

[28] A. Baldansuren and E. Roduner, Chem. Phys. Lett. 2009, **473**, 135-137.

[29] J. Michalik, Appl. Magn. Reson., 1996, **10**, 507-537.

[30] J. Michalik, L. Kevan, J. Am. Chem. Soc. 1986, **108**, 4247-4253.

[31] J. Michalik, J. Sadlo, T. Kodaira, S. Shimomura, H. Yamada, J. Radioanal. Nucl. Chem. 1998, **232**, 135-137.

[32] J. Michalik, A. Van der Pol, E. J. Reijerse, T. Wasowicz, E. De Boer, Appl. Magn. Reson. 1992, **3**, 19-35.

[33] J. Michalik, T. Wasowicz, J. Sadlo, E. J. Reijerse, L. Kevan, Radiat. Phys. Chem. 1996, **47**, 75-81.

[34] J. R. Morton, K. F. Preston, J. Magn. Reson., 1986, **68**, 121-128.

[35] M. Pereiro, D. Baldomir, J. E. Arias, Phys. Rev. A 2007, 75, 063204-1/063204-5

[36] T. Sun, K. Seff, Chem. Rev. 1994, **94**, 857-870.

[37] V. I. Bakhmutov, Chem Rev, 2011, **111**, 530-562.

[38] C. P. Grey, C. M. Dobson, A. K. Cheetham, R. J. B. Jakeman, J. Am. Chem. Soc. 1989, **111**, 505-511.

[39] C. P. Grey, M. E. Smith, A. K. Cheetham, C. M. Dobson, R. Dupree, J. Am. Chem. Soc. 1990, **112**, 4670-4675.

[40] G. Pintacuda, G. Kervern, Top. Curr. Chem. 2013, **335**, 157-200.

[41] N. E. Bogdanchikova, V. P. Petranovskii, R. Machorro M, Y. Sugi, V. M. Soto G, S. Fuentes M, Appl. Surf. Sci. 1999, **150**, 58-64.

[42] O. Y. Golubeva, N. Y. Ul'yanova, Glass Phys. Chem. 2015, **41**, 537-544.

[43] M. Matsuoka, W.-S. Ju, H. Yamashita and M. Anpo, J. Photochem. Photobiol. A 2003, **160**, 43-46.

[44] K. Sato, T. Yoshinari, Y. Kintaichi, M. Haneda, H. Hamada, Appl. Catal., B 2003, **44**, 67-78.

[45] A. Satsuma, J. Shibata, K.-I. Shimizu, T. Hattori, Catal. Surv. Asia 2005, **9**, 75-85.

[46] P. Sazama, L. Capek, H. Drobna, Z. Sobalik, J. Dedecek, K. Arve, B. Wichterlova, J. Catal. 2005, **232**, 302-317.

[47] J. Shibata, Y. Takada, A. Shichi, S. Satokawa, A. Satsuma, T. Hattori, J. Catal. 2004, **222**, 368-376.

[48] B. Wichterlova, P. Sazama, J. P. Breen, R. Burch, C. J. Hill, L. Capek, Z. Sobalik, J. Catal. 2005, **235**, 195-200.

[49] S. Dzwigaj, N. Popovych, P. Kyriienko, J-M. Krafft, S. Soloviev, Micropor. Mesopor. Mater. 2013, **189**, 16-24.

[50] M. Boutros, J.M. Trichard, P. Da Costa, Appl. Catal. B 2009, **91**, 640-648.

[51] J. J. van der Klink, H. B. Brom, Prog. Nucl. Magn. Reson. Spectrosc. 2000, **36**, 89-201.

[52] J. K. Plischke, A. J. Benesi, M. A. Vannice, J. Phys. Chem. 1992, **96**, 3799-3806.

[53] K. Son, Z. Jang, J. Korean Phys. Soc. 2013, **62**, 292-296.

[54] K. Hadjiivanov, G.N. Vayssilov, Adv. Catal. 2002, **47**, 307–511.

[55] Y.Y. Huang, J. Catal. 1974, **32**, 482-491.

[56] K. Hadjiivanov, H. Knözinger, J. Phys. Chem. B 1998, **102**, 10936-10940.

[57] G. Centi, G. Gollinetti, G. Busca, J. Phys. Chem. 1990, **94**, 6813–6819.

[58] G. Busca, G. Centi, F. Trifiro, V. Lorenzelli, J. Phys. Chem. 1986, **90**, 1337–1344.

[59] X. He, X. Huang, Z. Wang, Y. Yan, Micropor. Mesopor. Mater. 2011, **142**, 398-403.

[60] R. Zhang, Z. Wang, Chin. J. Chem. Eng. 2015, **23**, 1131–1137

Figure captions

Figure 1. XRD recorded at ambient atmosphere of SiBEA, $Ag_{3.0}$SiBEA, Red-C-$Ag_{3.0}$SiBEA, $Ag_{6.0}$SiBEA and Red-C-$Ag_{6.0}$SiBEA.

Figure 2. FTIR spectra recorded at 100 K of SiBEA and C-$Ag_{6.0}$SiBEA calcined at 773 K for 2 h in flowing 2.5 % O_2/Ar (50 mL min^{-1}) and then outgassed at 573 K (10^{-3} Pa) for 1 h.

Figure 3. Photoluminescence spectra of SiBEA and $Ag_{3.0}$SiBEA with the excitation of 250 nm.

Figure 4. The excitation spectra of SiBEA and $Ag_{3.0}$SiBEA monitored at 400 nm emission light.

Figure 5. ^{109}Ag MAS NMR spectra of $Ag_{3.0}$SiBEA, $Ag_{6.0}$SiBEA and Red-C-$Ag_{6.0}$SiBEA recorded at room temperature and MAS frequency of 14 kHz

Figure 6. EPR spectra recorded at 77 K of $Ag_{3.0}$SiBEA (a), C-$Ag_{3.0}$SiBEA (b) and Red-C-$Ag_{3.0}$SiBEA (c) samples.

Figure 7. EPR spectra recorded at 77K of $Ag_{6.0}$SiBEA (a), C-$Ag_{6.0}$SiBEA (b) and Red-C-$Ag_{6.0}$SiBEA (c) samples.

Figure 8. DR UV-vis spectra recorded at ambient atmosphere of as prepared and reduced $Ag_{3.0}$SiBEA and $Ag_{6.0}$SiBEA.

Figure 9. XP spectra recorded at room temperature of Ag 3d of calcined $Ag_{3.0}$SiBEA and $Ag_{6.0}$SiBEA.

Figure 10. TEM image and diffraction patterns of Red-C-$Ag_{3.0}$SiBEA.

Figure 11. FTIR difference spectra (OH stretching range) recorded at room temperature of C-$Ag_{6.0}$SiBEA (calcined at 773 K for 2 h in flowing 2.5 % O_2/Ar (50 mL min^{-1}), outgassed at 573 K (10^{-3} Pa) for 1 h after adsorption of CO at 100 K: equilibrium CO pressure of 100 Pa (a) and development of the spectra during evacuation at 100 K (b–e)).

Figure 12. FTIR difference spectra (carbonyl stretching region) recorded at room temperature of C-$Ag_{6.0}$SiBEA (calcined at 773 K for 2 h in flowing 2.5 % O_2/Ar (50 mL min^{-1}), outgassed at 573 K (10^{-3} Pa) for 1 h after adsorption of CO at 100 K: equilibrium CO pressure of 100 Pa (a) and development of the spectra during evacuation at 100 K (b–e)).

Figure 13. FTIR difference spectra recorded at room temperature of SiBEA, $Ag_{3.0}$SiBEA and $Ag_{6.0}$SiBEA after calcination at 773 K, 1 h in O_2 ($2 \cdot 10^4$ Pa), outgassing at 10^{-3} Pa for 1 h at 673 K, adsorption of pyridine and desorption of pyridine at 423 K.

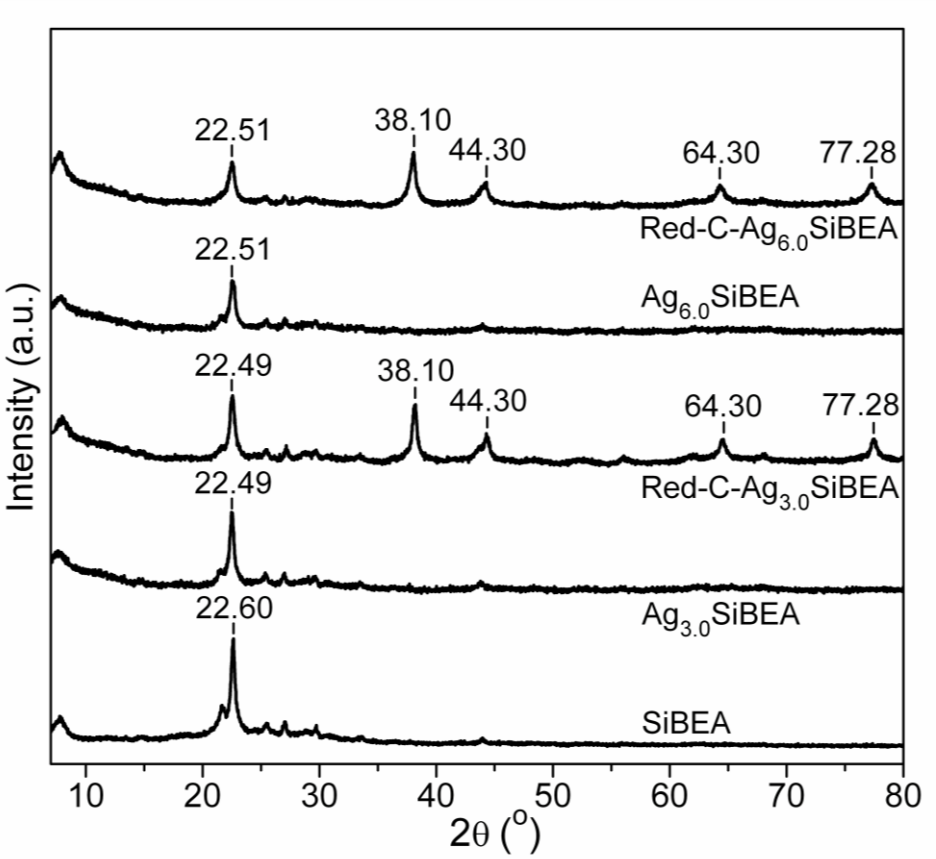
22.51
38.10
44.30
64.30
77.28
Red-C-Ag6.0SiBEA
22.51
Ag6.0SiBEA
22.49
38.10
44.30
64.30
77.28
Red-C-Ag3.0SiBEA
22.49
Ag3.0SiBEA
22.60
SiBEA
Intensity (a.u.)
10
20
30
40
50
60
70
80
2θ (°)

Figure 1

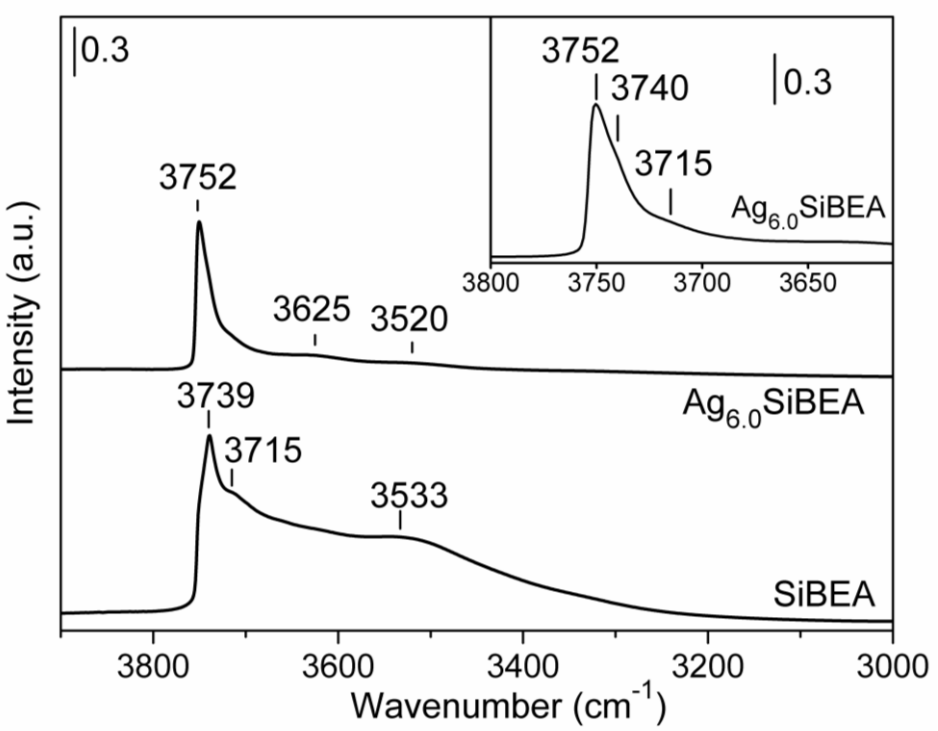
0.3
3752
3740
3715
Ag6.0SiBEA
3800
3750
3700
3650
3752
3625
3520
Ag6.0SiBEA
3739
3715
3533
SiBEA
Intensity (a.u.)
3800
3600
3400
3200
3000
Wavenumber (cm-1)

Figure 2

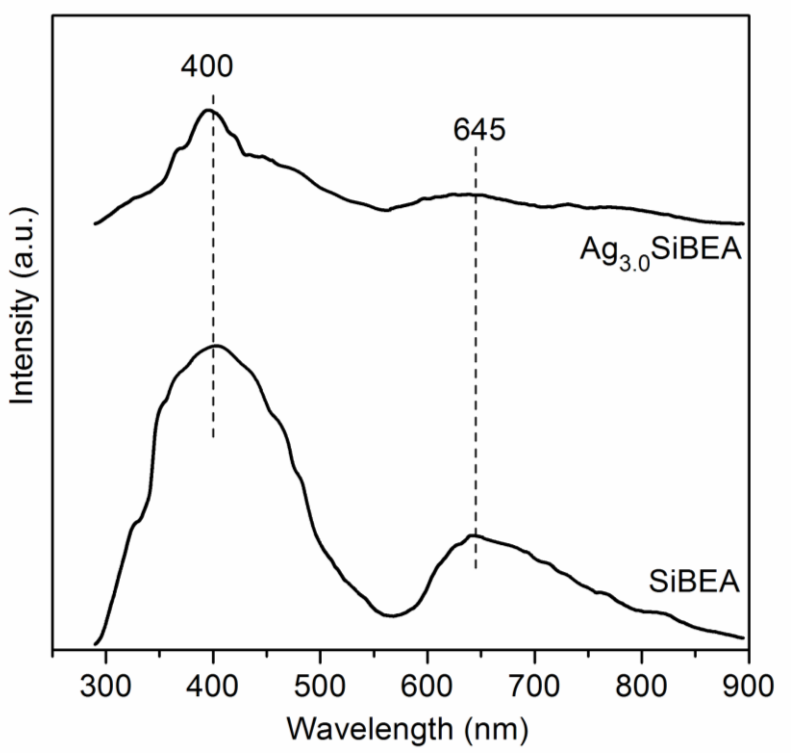
400
645
Ag3.0SiBEA
SiBEA
Intensity (a.u.)
300
400
500
600
700
800
900
Wavelength (nm)

Figure 3

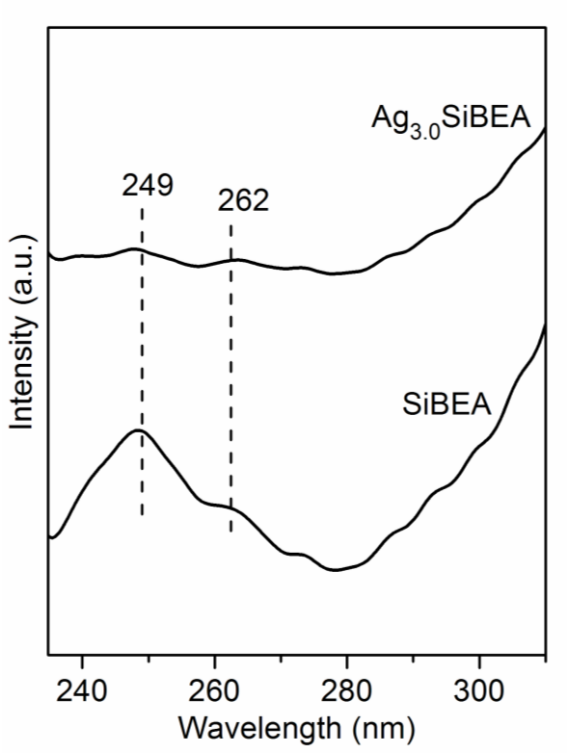
Ag3.0SiBEA
249
262
SiBEA
Intensity (a.u.)
240
260
280
300
Wavelength (nm)

Figure 4

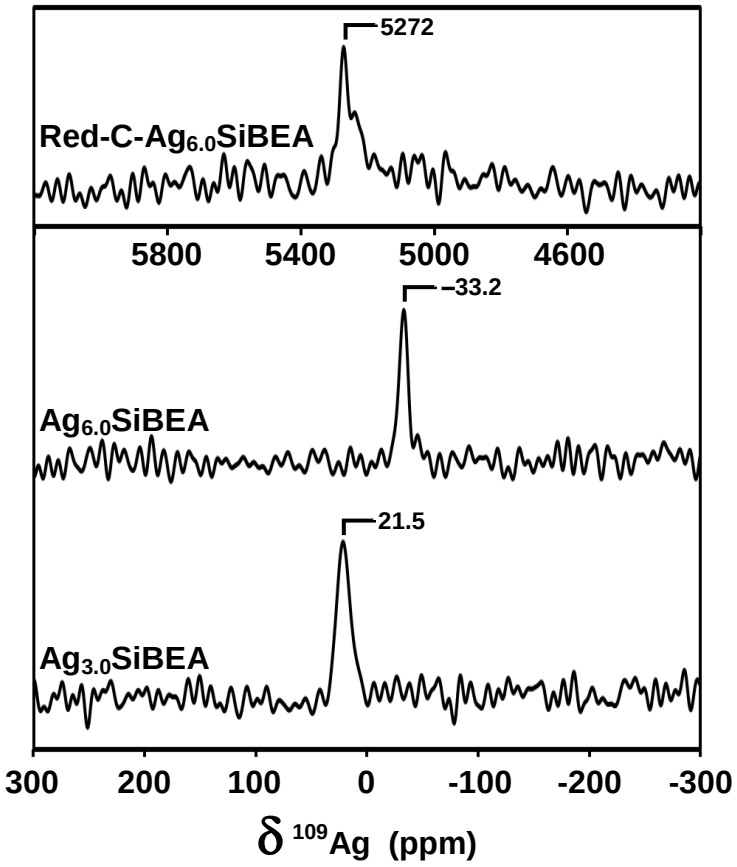
5272
Red-C-Ag6.0SiBEA
5800
5400
5000
4600
–33.2
Ag6.0SiBEA
21.5
Ag3.0SiBEA
300
200
100
0
-100
-200
-300
δ 109Ag (ppm)

Figure 5

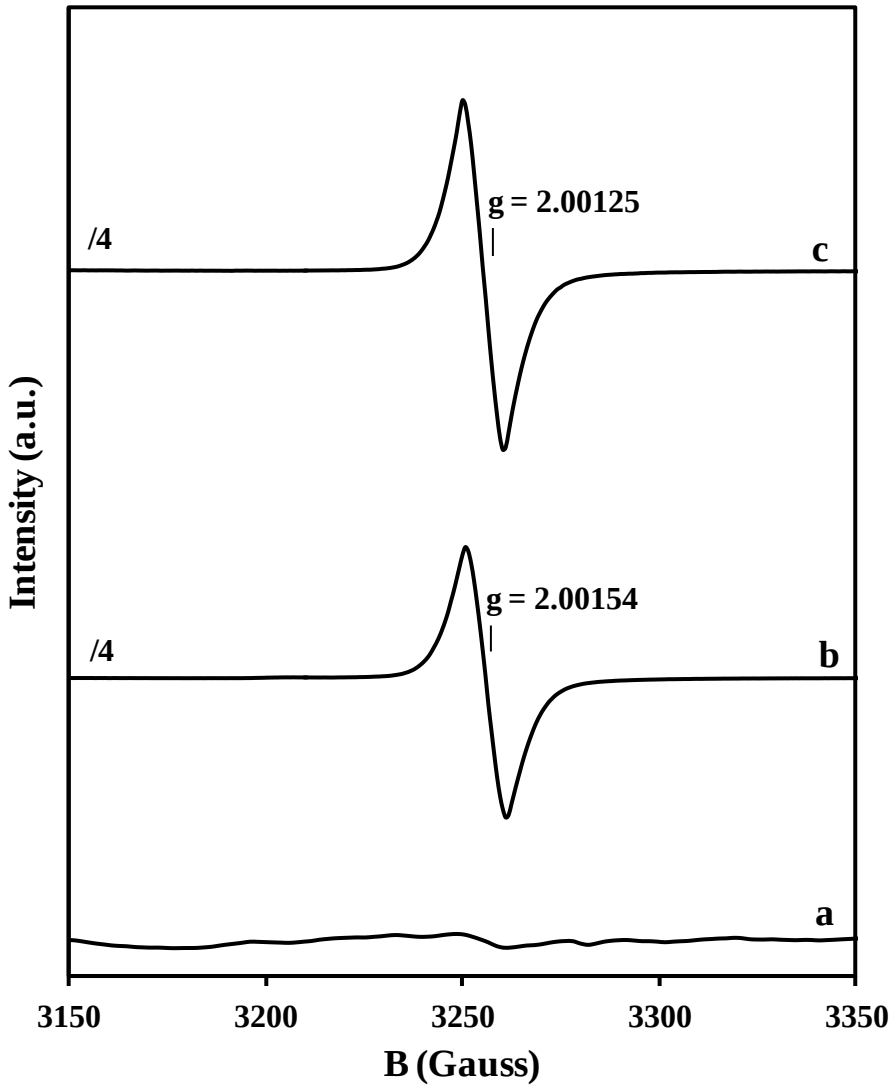
g = 2.00125
/4
c
Intensity (a.u.)
g = 2.00154
/4
b
a
3150
3200
3250
3300
3350
B (Gauss)

Figure 6

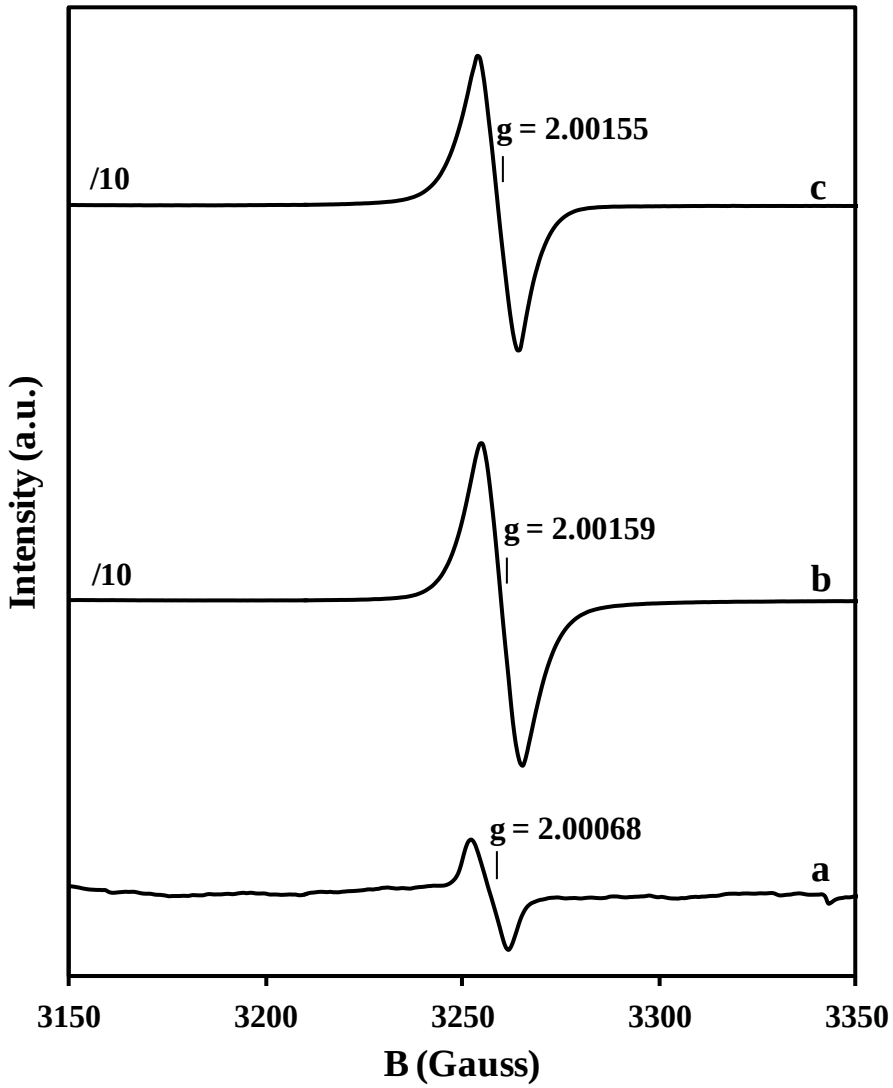
g = 2.00155
/10
c
g = 2.00159
/10
b
g = 2.00068
a
Intensity (a.u.)
3150
3200
3250
3300
3350
B (Gauss)

Figure 7

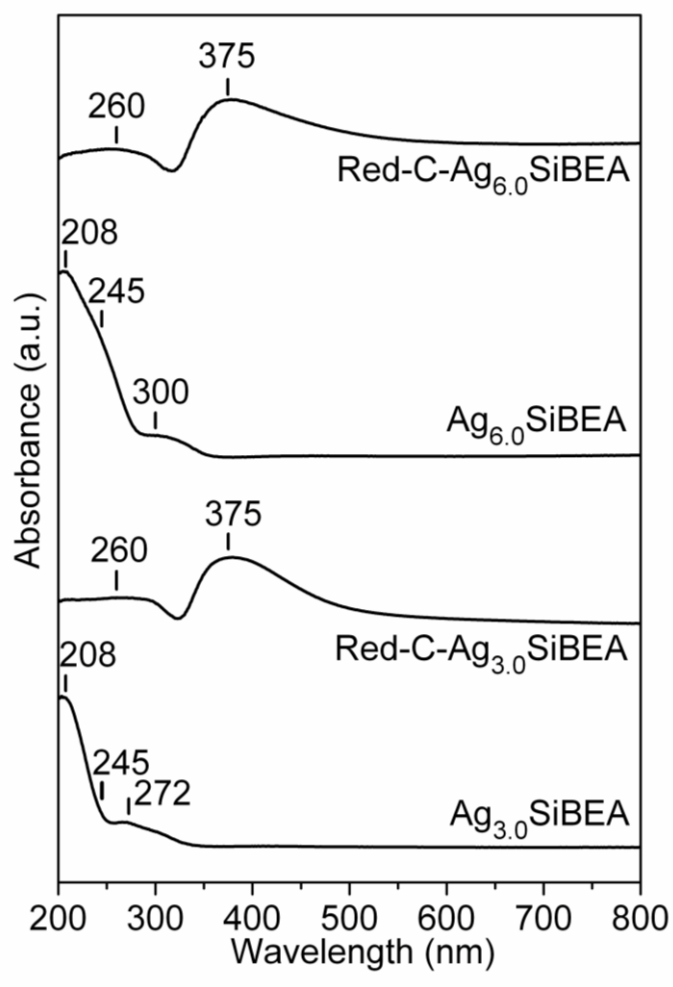
375
260
Red-C-Ag6.0SiBEA
208
245
300
Ag6.0SiBEA
375
260
Red-C-Ag3.0SiBEA
208
245
272
Ag3.0SiBEA
Absorbance (a.u.)
200
300
400
500
600
700
800
Wavelength (nm)

Figure 8

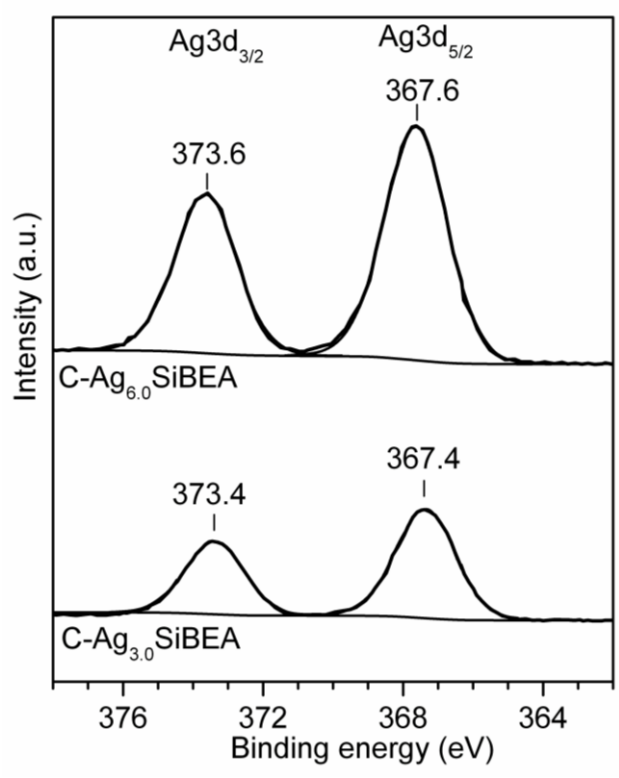
Ag3d3/2
Ag3d5/2
367.6
373.6
Intensity (a.u.)
C-Ag6.0SiBEA
367.4
373.4
C-Ag3.0SiBEA
376
372
368
364
Binding energy (eV)

Figure 9

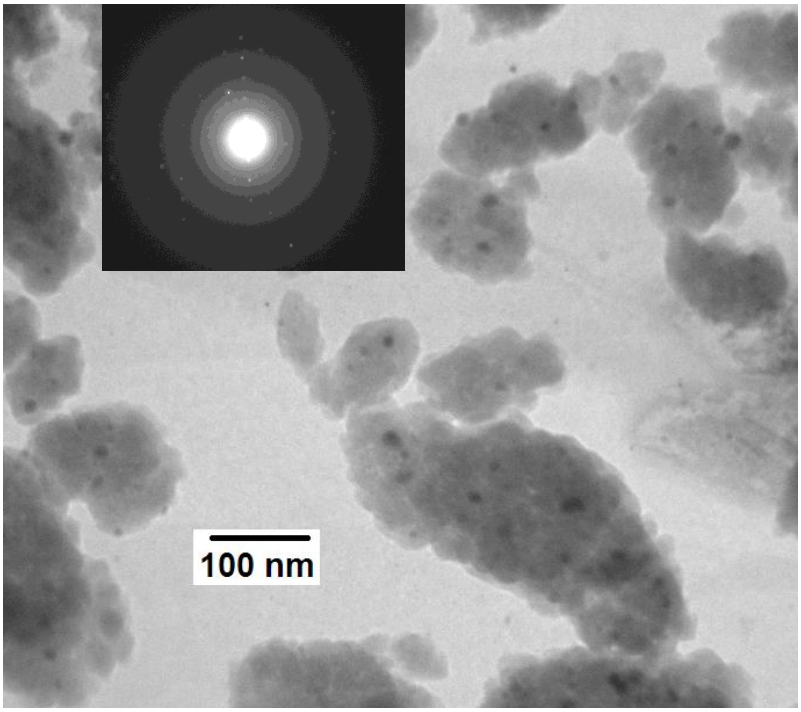

Figure 10

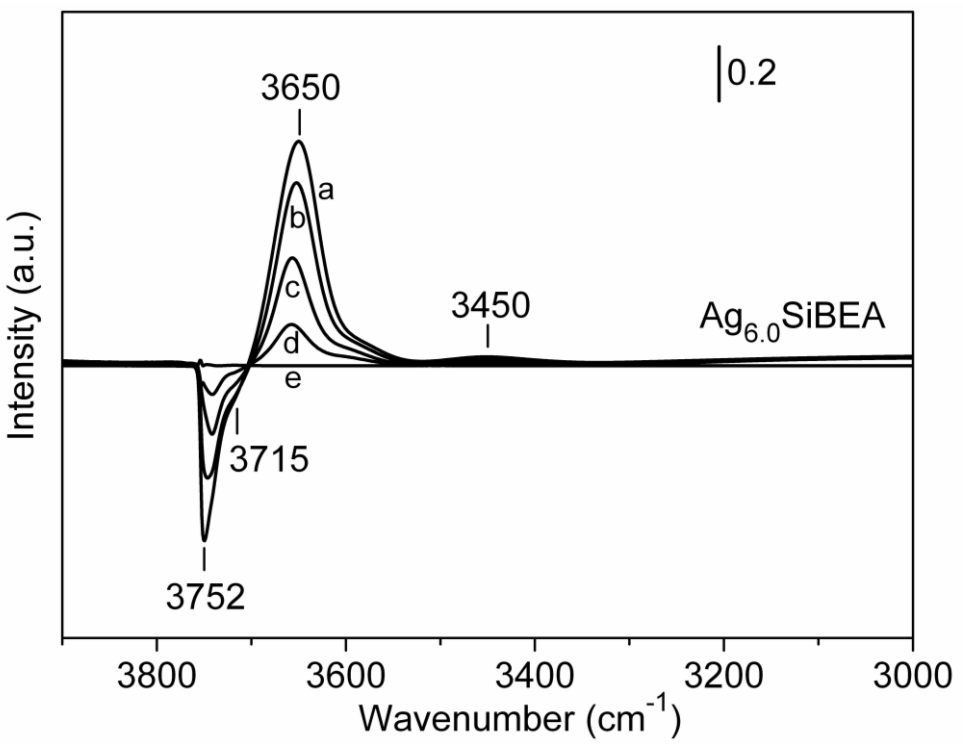
0.2
3650
a
b
c
d
e
3450
Ag6.0SiBEA
3715
3752
Intensity (a.u.)
3800
3600
3400
3200
3000
Wavenumber (cm-1)

Figure 11

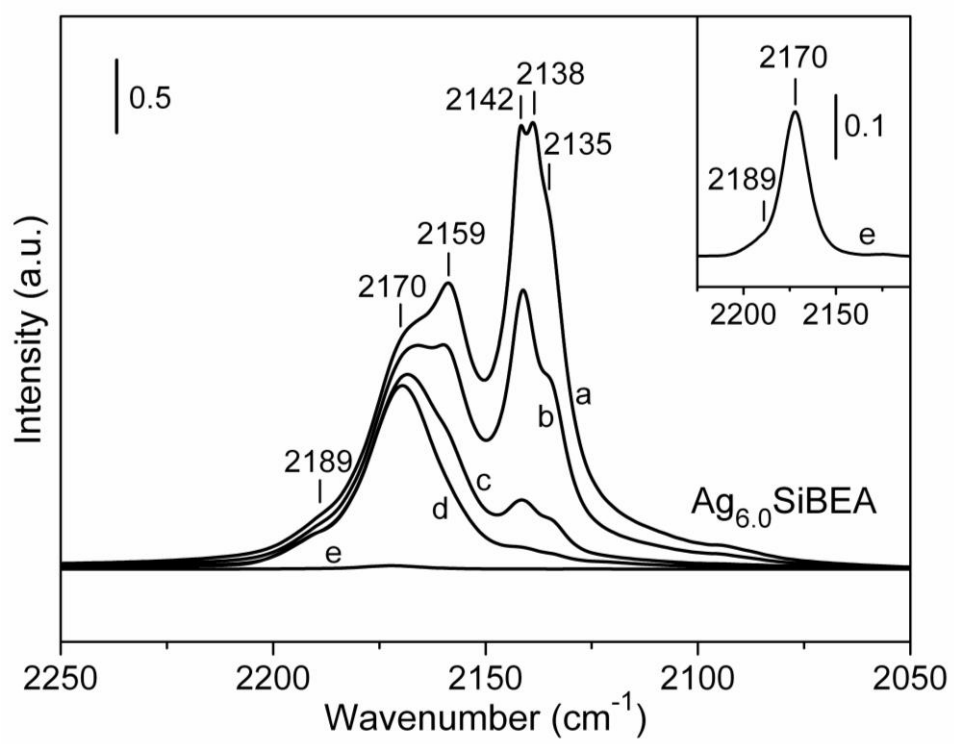
0.5
2138
2142
2135
2159
2170
2189
a
b
c
d
e
Ag6.0SiBEA
Intensity (a.u.)
2250
2200
2150
2100
2050
Wavenumber (cm-1)
2170
0.1
2189
e
2200
2150

Figure 12

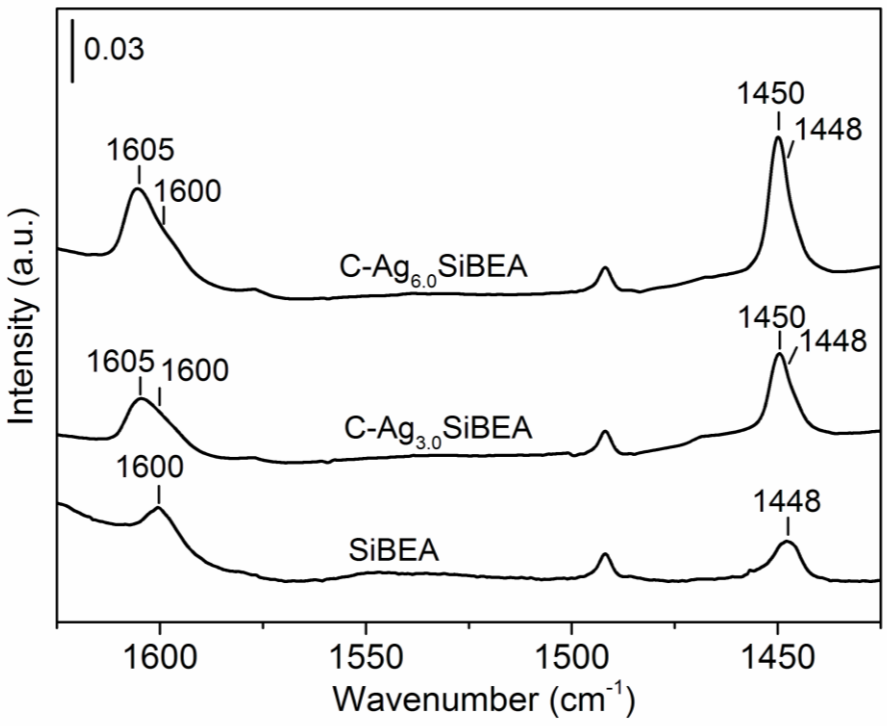
0.03
1450
1448
1605
1600
C-Ag6.0SiBEA
1450
1448
1605
1600
C-Ag3.0SiBEA
1600
1448
SiBEA
Intensity (a.u.)
1600
1550
1500
1450
Wavenumber (cm-1)

Figure 13